Physical Priors in Virtual Colonoscopy*

Hassan Rivaz[a], Yoshihisa Shinagawa[b], Jianming Liang[c]

[a] ERC for Computer Integrated Surgery, Johns Hopkins University, Baltimore, MD, rivaz@jhu.edu
[b] Siemens Medical Solutions USA, Inc., Malvern, PA, yoshihisa.shinagawa@siemens.com
[c] Arizona State University, Phoenix, AZ, jianming.liang@asu.edu

ABSTRACT

Electronic colon cleansing (ECC) aims to remove the contrast agent from the CT abdominal images so that a virtual model of the colon can be constructed. Virtual colonoscopy requires either liquid or solid preparation of the colon before CT imaging. This paper has two parts to address ECC in both preparation methods. In the first part, meniscus removal in the liquid preparation is studied. The meniscus is the curve seen at the top of a liquid in response to its container. Left on the colon wall, the meniscus can decrease the sensitivity and specificity of virtual colonoscopy. We state the differential equation that governs the profile of the meniscus and propose an algorithm for calculating the boundary of the contrast agent. We compute the surface tension of the liquid-colon wall contact using in-vivo CT data. Our results show that the surface tension can be estimated with an acceptable degree of uncertainty. Such an estimate, along with the meniscus profile differential equation will be used as an a priori knowledge to aid meniscus segmentation. In the second part, we study ECC in solid preparation of colon. Since the colon is pressurized with air before acquisition of the CT images, a prior on the shape of the colon wall can be obtained. We present such prior and investigate it using patient data. We show the shape prior is held in certain parts of the colon and propose a method that uses this prior to ease pseudo-enhancement correction.

Keywords: Virtual colonoscopy, electronic colon cleansing, CT colonography, meniscus, unprepared colon

1. INTRODUCTION

Colon cancer is the second deadliest cancer in the US [1]. Worldwide, it accounts for 945,000 new cases and 500,000 deaths each year [1]. Most colon cancers begin as benign polyps that can be found by colonoscopy. Optical colonoscopy is considered the gold standard for finding polyps and involves passing an endoscope through rectum and screening colon. The incident of colon cancer can be reduced by polypectomy using colonoscopy screening [2]. However, optical colonoscopy requires sedation and is an invasive procedure

CT colonography (CTC) is a rapidly evolving non-invasive alternative for optical colonoscopy for detecting polyps [3,4,5,6]. The American Cancer Society (ACS) has most recently added CTC study to its screening guidelines for colorectal cancer. Recently, several large-scale multi-center clinical trials (ACRIN, IMPACT, etc) for virtual colonoscopy have successfully finished, demonstrating the sensitivity of CTC in the detection of polyps on a par with that of optical colonoscopy. These trials validated the clinical use of CTC for early detection of colon cancer in screening population, thus bringing CTC to a new exciting era.

In a common clinical practice, oral contrast agents are included in patient's diet along with high amount of liquid just hours before the scan. Laxative drugs are also administrated before the scan to minimize the amount of residual stool. We refer to this method as *liquid preparation*. An efficient electronic colon cleansing (ECC) method is therefore essential for removing residual fecal materials for visualizing the entire colonic mucosa and for Computer Aided Detection (CAD) of polyps in the colon. Different approaches have been taken towards ECC. A probabilistic method with special regularization through Markov random field is utilized in [4,5]. Fuzzy clustering and deformable models are

* This work was carried out at Siemens Medical Solutions USA, Inc., Malvern, PA

Medical Imaging 2009: Computer-Aided Diagnosis, edited by Nico Karssemeijer, Maryellen L. Giger
Proc. of SPIE Vol. 7260, 726019 · © 2009 SPIE · CCC code: 1605-7422/09/$18 · doi: 10.1117/12.813554

utilized in [8,9]. A low level classification based on statistical analysis of intensity values of 3D neighborhood of each voxel is used in [10], followed by a high level processing technique to extract colon lumen. Different artifacts caused by the contrast agent have also been considered. For example, the residual enhancement (*pseudo-enhancement*) of the contrast agent on the colon wall caused by scattering of photons is corrected in [11].

Unfortunately liquid preparation requires physical colon cleansing. Fecal tagging of the unprepared colon has been proposed as a method to reduce discomfort, side effects and sleep disturbance of bowel preparation [1]. We refer to this method as either *solid colon preparation* or *unprepared colon CTC*, which does not require use of laxative drugs. Recent study has shown that ECC can increase the sensitivity and specificity of the CT colonography with solid preparation [15]. Previous research on ECC for solid preparation is limited. Carston et al [14] propose an iterative algorithm for stool subtraction, which successfully eliminates untagged parts of the stool. However, it removes colon folds in the ECC process, impairing the visualization and polyp detection.

In this paper, we address the ECC in both preparation methods. In the liquid preparation, physics of the meniscus caused by surface tension is explained and the differential equation governing its shape is derived. Some preliminary results verifying the approach with patient CT data with liquid preparation is provided. In the solid preparation, we propose an ECC framework with three major steps: (1) removing untagged parts of the stool, (2) removing the air-stool partial volume and (3) reconstructing tissue-stool boundary considering the pseudo-enhancement artifact. We propose a method to find the extent of the effect of the pseudo-enhancement. The incorporation of this method into a pseudo-enhancement correction algorithm is the subject of future work.

2. MENESCUS SHAPE PRIOR

Meniscus is the curve in the surface of a liquid and is produced because the liquid molecules have a different attraction to each other than to the container. In [3], the artifact caused by meniscus is referred to as residue that remains in tub after bath (Figure 1 (a) & (b)). Left on the colon after ECC, meniscus impairs the 3D visualization and can be misleading to the radiologist or to the computer aided detection technique. In our colon CAD (computer aided diagnosis) system, a large number of false positives are generated in the initial candidate generation phase. Knowledge of the shape of the meniscus can help to design algorithms to remove this type of false positives. Such knowledge can also improve ECC for visualization. The evolution of the meniscus shape is still an unanswered question [12]. To simplify the problem, we assume steady state condition and derive the differential equation that governs the shape of the meniscus. We then examine the differential equation on the experimental data. The prior of the shape of the meniscus can be utilized in two important applications: (1) to enhance 3D visualization, and (2) to improve the sensitivity and specificity of colon CAD systems.

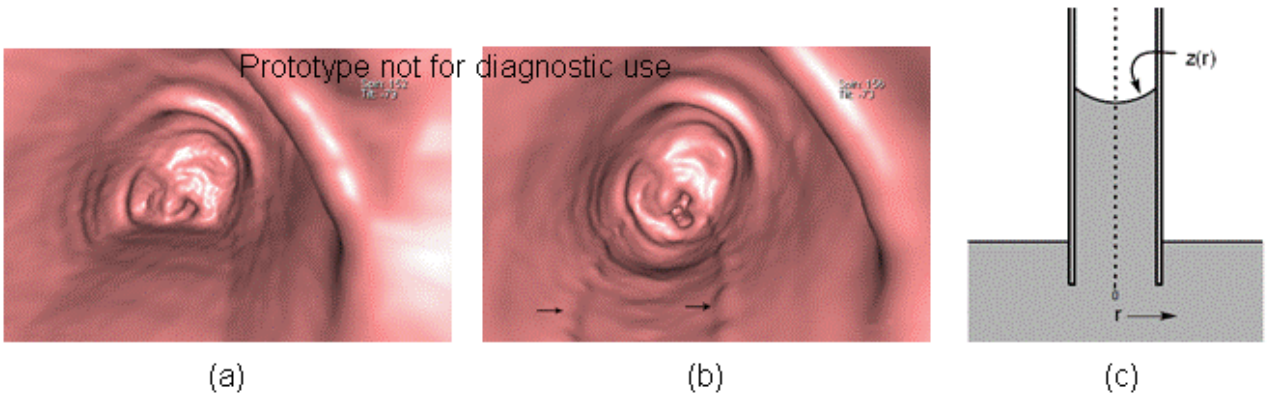

Fig. 1. (a) & (b) Uncleansed and cleansed images respectively. Characteristic linear artifact where air-fluid level interfaces with colon wall (arrows in (b)) has been likened to residue that remains in tub after bath. (c) Capillary rise of a liquid.

2.1 Meniscus Shape Profile

For very narrow tubes (up to 2mm in diameter for water in glass tube), the shape of the meniscus is assumed to be spherical. For larger tubes the meniscus has a complicated shape. At a point with distance r from the center (Fig. 1 (c)), we have

$$\Delta p(r) = \gamma\left(\frac{1}{R_1} + \frac{1}{R_2}\right) = \gamma\left(\frac{z''}{(1+z'^2)^{3/2}} + \frac{z'}{r(1+z'^2)^{1/2}}\right) \qquad (1)$$

where $\Delta p(r)$ is the pressure difference caused by the curvature of the meniscus surface, R_1 and R_2 are local radii of the meniscus surface in two dimensions, γ is the surface free energy in the solid-liquid interface[†] and the differentiation is performed with respect to r. This equation states that the pressure difference induced by the curvature of a liquid is proportional to its local curvature. Substituting $\Delta p(r) = \rho g z(r)$ where ρ is the density of the liquid and g is the acceleration due to gravity, we have [12]

$$z = \frac{\gamma}{\rho g}\left(\frac{z''}{(1+z'^2)^{3/2}} + \frac{z'}{r(1+z'^2)^{1/2}}\right) \qquad (2)$$

which determines the shape of the meniscus given the boundary conditions. This differential equation is valid even if the container wall is not vertical.

2.2 Edge Detection

The boundary between the tagged material and air should be calculated with subpixel accuracy. Such accuracy is required for calculating the first and second order derivatives in equation (2). We apply a simple recursive algorithm for edge detection as follows:

1. A Gaussian smoothing is applied to the image followed by gradient calculation in the z and r directions, resulting in I_z and I_r respectively. $I_{zr} = (I_z^2 + I_r^2)^{1/2}$ is calculated from I_z and I_r.
2. A binary mask M is calculated according to the steps a and b below. Nonzero pixels of the mask encompass the boundary between the tagged material and air.
    a. The air is found by a simple semi-automatic region growing technique where the seed is manually placed.
    b. The liquid-air boundary is characterized by high *negative* gradient in the z direction. The mask is found by thresholding I_z and eliminating the ones in the mask that are not below air. The mask is shown in Figure 2 (a). The mask contains about 5 nonzero elements at each r (the width of the mask in Figure 2 (a)).
3. The boundary with subpixel accuracy is found by calculating the first moment of the weighted gradient image $w.I_{zr}$ along vertical lines (constant r), where $w = e^{\left(\frac{z-z_0}{\sigma}\right)^2}$ is an exponential weight with $z_0 = z_0(r)$ as the center line of the mask M at the corresponding vertical line (constant r). We set $\sigma = 2$ pixels. The resulting boundary is shown in Figure 2 (b), superimposed on the CT image.
4. The discontinuities in the mask are carried over to the boundary resulting in non-smooth result (Figure 2 (b)). To overcome this problem, the algorithm returns to step 3 with the new boundary used for $z_0 = z_0(r)$ (no new mask is created since only the centerline is required for computing w).
5. The algorithm stops iterating when the boundary stops changing considerably. The final boundary is shown in Figure 2 (c) which is obtained after 24 iterations.

[†] Accurately speaking, γ is the difference in surface free energy between the solid-gas interface and the solid liquid interface.

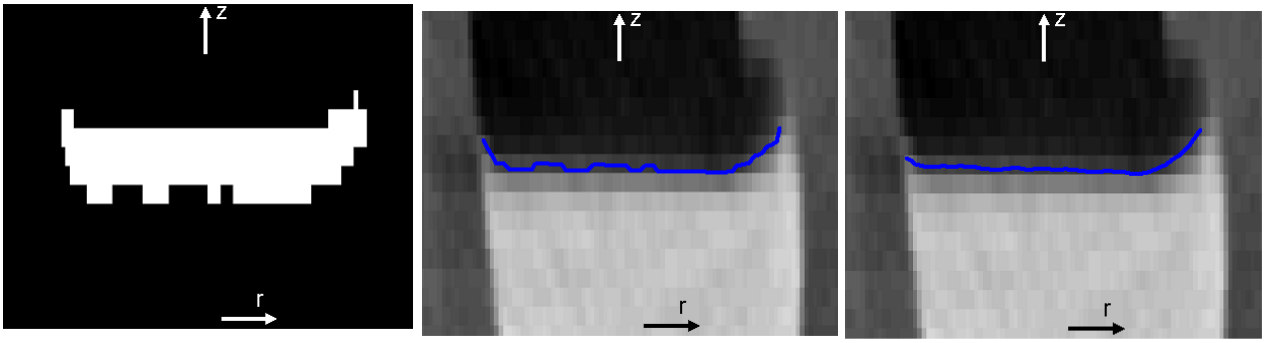

(a) (b) (c)

Fig. 2. (a) Binary mask M created by thresholding the vertical gradient I_z. Tagged material is in below the mask and air is on top of it. (b) The resulting boundary calculated from I_{zr} using the binary mask and the exponential weight w in the first iteration (c) Final boundary results after 24 iterations.

An important feature of the algorithm is that the final result is independent of the initial threshold: although different thresholds result in different masks M in the beginning, the boundary converges to the same result after few iterations. Figure 2 (a) shows the first iteration of the subpixel boundary generated from two different masks M corresponding to two different thresholds. Since the masks are different, the resulting subpixel boundaries are also different. Figure 2 (b) & (c) show the boundary in the second and third iterations. The two boundaries are converging to the same result. Figure 2 (d) shows the boundary at the eighth iterations, where the two boundaries converge. The dashed line corresponds to the mask M which is obtained with a smaller threshold. Therefore, the detected boundary is one pixel longer in the right.

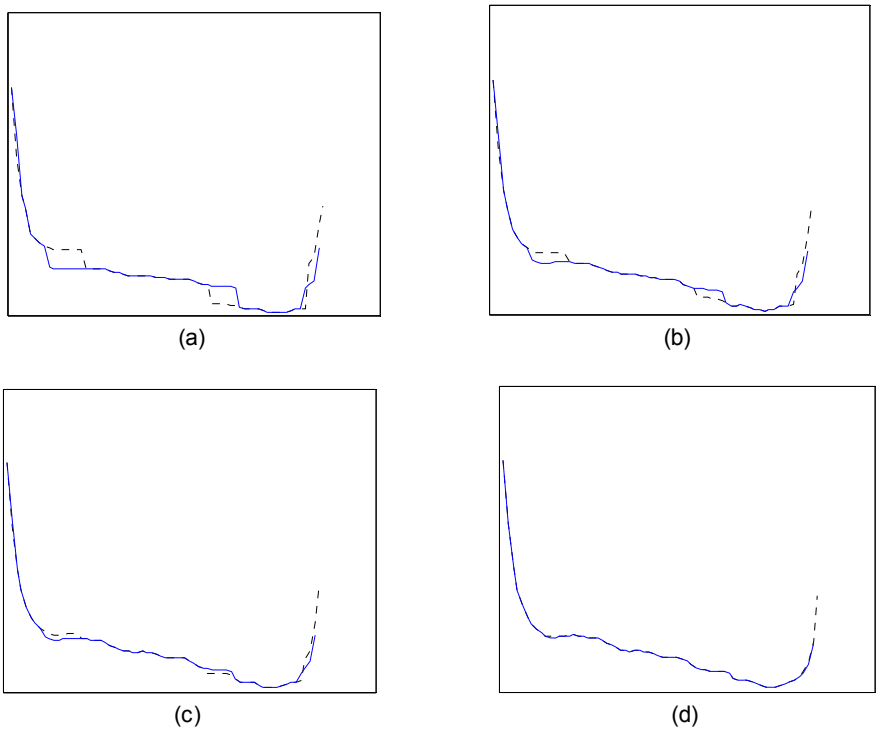

(a) (b) (c) (d)

Fig. 3. (a) – (d) respectively correspond to the calculated boundary at 1st, 2nd, 3rd and 8th iterations. The corresponding binary masks M of the two solid and dotted lines are obtained with different thresholds (the solid line corresponds to a mask obtained with larger threshold).

2.3 Meniscus Prior Validation Results

The calculated boundary is then inserted into equation (2) to calculate the unknown coefficient $\gamma/\rho g$. The first derivative z' is calculated by forward differencing z and the second derivative z'' is calculated by backward differencing z'. The coefficient can be computed using all the pixels on the meniscus profile. Figure 4 (a) shows the computed $\gamma/\rho g$ from 35 CT slices. At the end of the meniscus profile (where it touches the container wall) the calculated boundary is not accurate because the tagged material is very thin in this region. Therefore, solving equation (2) for γ/ρg is not robust. Also at its beginning (where it starts rising from the liquid surface), the z, z' and z'' values are very small and again γ/ρg estimate is not consistent. Limiting the computation to the two middle points of the meniscus profile results in a more consistent $\gamma/\rho g$ estimate (Figure 4 (b)). The $\gamma/\rho g$ parameter is estimated to be around 5 from Figure 4(b).

We repeated the experiment for CT images obtained from 20 other patients. Similar results were obtained for the $\gamma/\rho g$ parameter. Such consistency indicates that the differential equation (2) along with the estimated surface tension parameter can be useful as an *a priori* knowledge for meniscus segmentation, where image data alone can contain substantial noise. Having the *a priori* knowledge of meniscus profile, development of an ECC method without the artifact of Figure 1 (b) is underway.

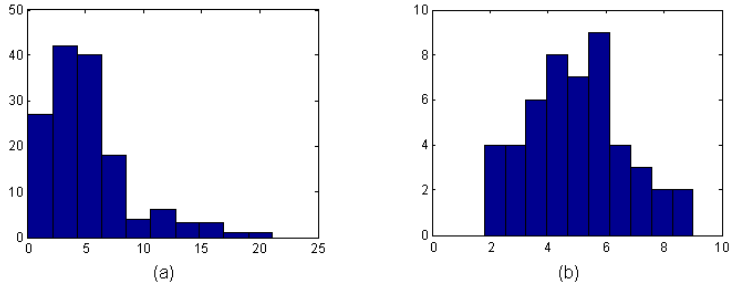

Fig. 4. The coefficient γ/ρg histograms calculated from (a) all points of the curved part of the boundary (starting from the top point of the meniscus extending for 5 pixels) and (b) the middle two points of the boundary (3 to 4 pixels away from the top point of the meniscus).

3. ECC IN UNPREPARED COLON

CTC without colon preparation does not require use of laxative drugs and is therefore much more convenient than CTC with liquid preparation of colon. ECC of unprepared colon is challenging for multiple reasons. First, although the stool is tagged with high attenuation materials, some of its parts do not have high attenuation due to its high degree of heterogeneity. Therefore a simple thresholding algorithm leaves many parts of stool. Second, partial volume effect creates voxels with the attenuations similar to colon wall at the boundary of stool and air. And third, pseudo-enhancement increases the attenuation of tissue close to tagged material due to scattering of photons. A three-step method for ECC of unprepared colon is proposed in this section. We try to address each of these three challenges in each step.

3.1 Removing Untagged Parts Of The Stool

A binary volume B_1 with the same size as the CT volume is generated and all voxel values are initialized to zero. Voxels with intensity more than a threshold T_1 are set to one. Threshold T_1 is chosen to be 375HU, such that all the voxels with intensity of one correspond to properly tagged stool. A 3D flood fill operation is performed to remove the untagged parts of the stool. As a result, the icelands of low intensity voxels isolated inside the stool are removed, resulting in the binary volume B_2. Figure 5 (a) shows six CT slices of a patient with solid colon preparation. Figure 5 (b) shows the corresponding slices after removal of the tagged and untagged stool using B_2. The untagged parts of the colon that are contained in the tagged parts are removed.

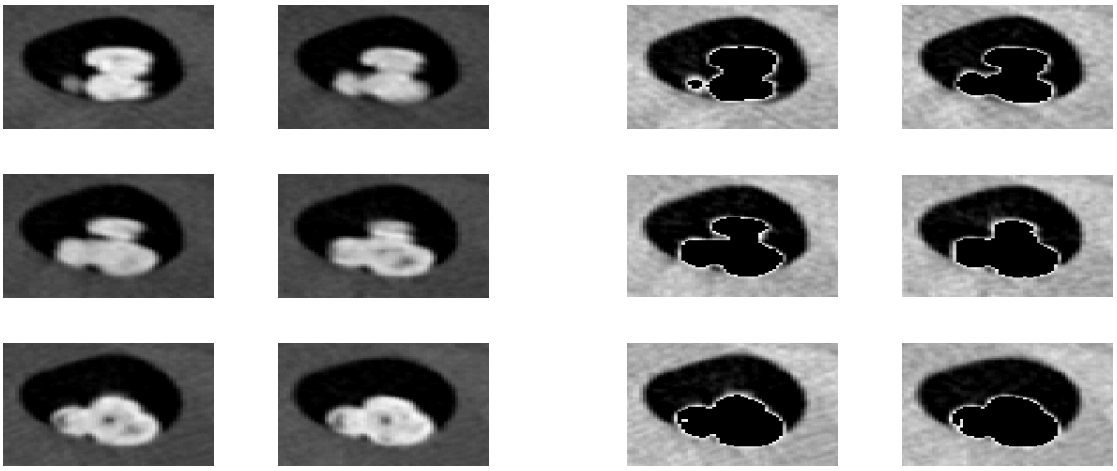

(a) (b)

Fig. 5. (a) Six CT consecutive slices with the tagged stool. (b) CT slices after removal of tagged and untagged stool.

3.2 Removing The Air-Stool Partial Volume (PV)

The air-stool boundary is identified as follws

1. The perimeter of the stool is found by morphological operations (subtracting B_2 from its dilation) on B_2.
2. Send 18 rays in 3D [16] out from each voxel on the boundary. Each ray 7 voxels long.
3. Pick 6 rays that go through maximum number of air voxels, i.e. voxels with attenuation less than -875HU.
4. If total percentage of air voxels in the 6 selected rays is more than 40%, add voxel to the mask B_2.
5. Repeat 3&4, but pick rays with maximum number of stool (>375HU) and add the voxel to the mask if stool voxels are more than 40%.
6. Iterate 1-5 for five times (PV thickness).
7. Remove any island in the air using 3D flood fill.

Step 5 is necessary for removal of parts of stool that are not tagged properly and are not contained in tagged stool (are close to the boundary of stool) and therefore are not removed after the 3D flood fill of Section 3.1. Figure 6 (a)-(c) show the CT slices corresponding to that of Figure 5 (b) after the 1st, 2nd and 3rd iterations of steps 1-5 respectively. Figure 6 (d) shows the corresponding CT slices after completion of step 7.

Figure 7 and 8 show how the method performs at colon folds. While most of the tagged material is removed, folds are remained intact after detagging. A final step that reconstructs the parts of the colon wal that is in touch with tagging material will complete ECC.

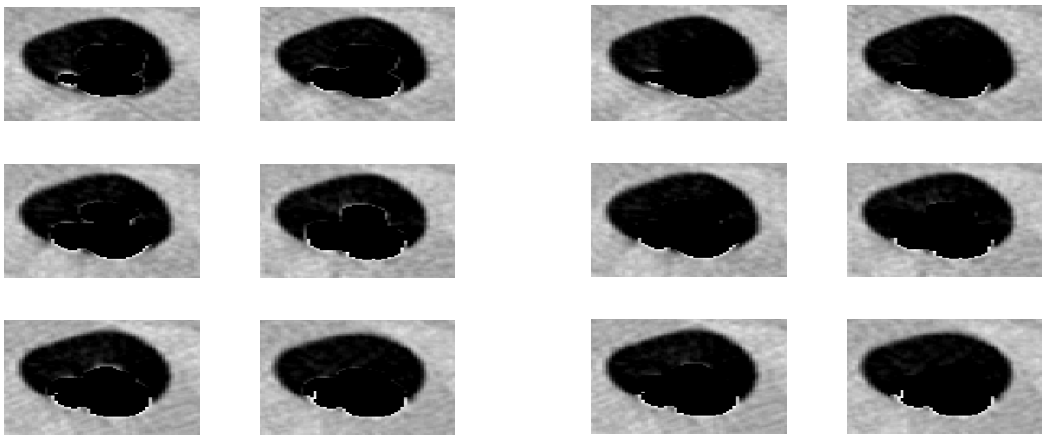

(a) (b)

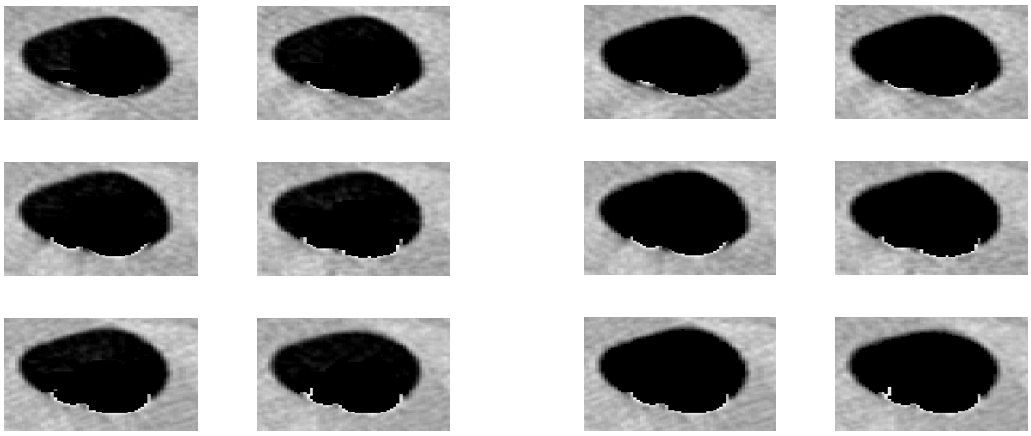

(c) (d)

Fig. 6. (a)-(c) The CT slices corresponding to that of Figure 5(b) after the 1st, 2nd and 3rd iterations of steps 1-5 respectively for removing air-stool PV. (d). The corresponding CT slices after completion of step 7.

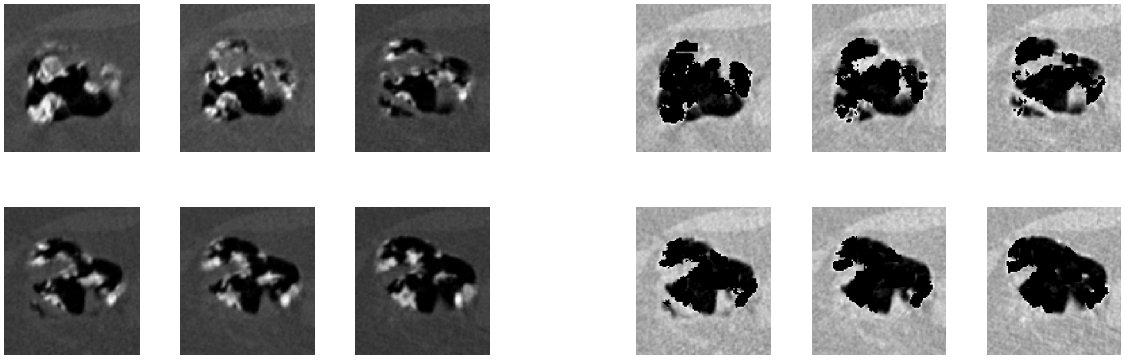

(a) (b)

Fig 7. (a) Colon folds covered with stool. (b) Results of removing stool after completion of step 7.

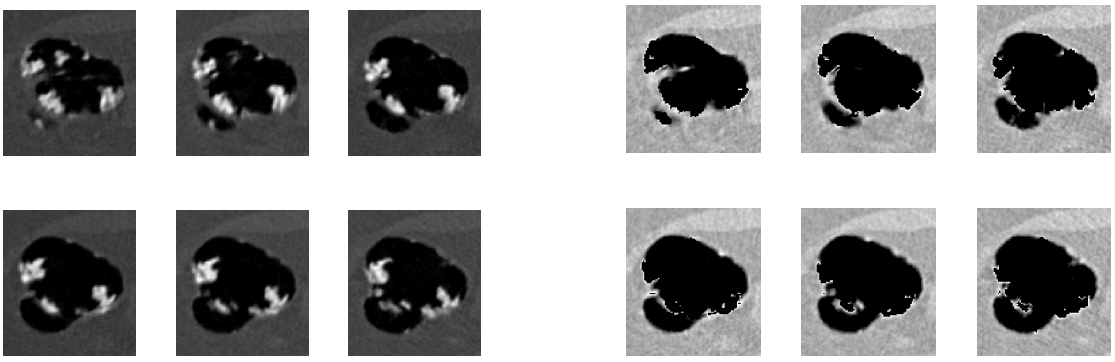

(a) (b)

Fig 8. (a) Colon folds covered with stool. (b) Results of removing stool after completion of step 7.

3.3 Measuring Pseudo-Enhancement

The tagging material artificially enhances the attenuation of nearby tissue in CT imaging. This pseudo-enhancement might hide polyps covered with tagged materials. Nappi and Yoshida [17] have proposed an iterative approach for correcting pseudo-enhancement. At each iteration, it is assumed that voxels with attenuation of more than some threshold artificially enhance the attenuation of their neighboring voxels. The enhancement is a Gaussian function of the distance of the neighboring voxel. Residual enhancement effect calculated at each iteration causes some additional enhancement, which is taken into account in the next iteration. The correction algorithm is shown to improve the ECC results visually. It is also shown to be effective in improving CAD performance.

The variance of the Gaussian function, however, is different for tagging materials with different attenuation and also depends on the CT machine. For calculating this variance, a phantom is filled in [17] with tagging materials with different attenuations and CT volumes of the phantom are obtained. A CT volume of the phantom without tagging material is also acquired to provide the reference for the calculation of the variance as a function of the attenuation of the tagging material. The need for fabrication and imaging a phantom is cumbersome. We call the procedure of the variance calculation "calibration".

In this section, we propose a phantomless calibration method for calculation of the variance of the pseudo-enhancement function. Our method uses the CT data obtained from the patient for calibration. It is based on the fact that colon is filled with pressured air during CT colonography. The deformation of the colon wall due to the air pressure depends on the pressure of the air. Since this pressure is constant across colon, a prior on the shape of the colon wall can be obtained.

Assuming the colon wall is homogeneus and thin, its average curvature H can be calculated from the air pressure P using $H = \alpha P$ where α depends on the mechanical properties of the colon wall and its thickness [18]. The average curvature of a 3D surface x known as a funcion of y and z can be estimated as [19]

$$2H = \frac{(1 + x_y{}^2)x_{zz} - 2x_y x_z x_{yz} + (1 + x_z{}^2)x_{yy}}{(1 + x_y{}^2 + x_z{}^2)^{3/2}} \qquad (3)$$

where x_y and x_{yy} are the first and second derivatives of x with respect to y, x_z and x_{zz} are the first and second derivatives of x with respect to z and x_{yz} is the second derivatives of x with respect to y and z.

As we mentioned, the constant curvature property is valid only if the colon wall is thin and homogenous. Therefore, one cannot expect the curvature to be constant at the parts of colon where folds exist. We use this prior only at fold-free parts of colon (which are manually selected from patient data at this stage but can be simply automized) to estimate the variance of the pseudo-enhancement function. We first examine the extent to which the curvature is constant. We then propose a method showing how this prior can be used to in calibration.

Our calibration algorithm is currently in 2D for simplicity: it assumes 2D curvature is constant. Although this is obviously not correct, we make this assumption for our first phantomless calibration algorithm. We test this assumption using the parts of colon wall that do not touch any tagging material. Figure 9 (a) shows a slice of colon CT which is detagged according to the algorithms proposed in Sections 3.1 and 3.2. The bottom part of the colon wall is in contact with tagged stool, which is clear because of the sharp drop of attenuation in this region. The blue curves show the subpixel boundary at the parts of the colon that do not touch tagged material. This boundary is calculated using an algorithm similar to the algorithm explained in Section 2.2. Axes x, y and z are shown: a subpixel value for x is know at each integer value of y and z. Figure 9 (b) shows the histogram of 2D and 3D curvatures calculated for each pixel on the boundary for multiple slices that do not contain folds. Variances of 2D and 3D curvature are 0.00254 and 0.00156 respectively, suggesting that 3D curvature is more preserved as expected. Assuming that curvature is constant in each slice we reconstruct the missing air-colon wall boundary, the part of the colon wall touching tagged material.

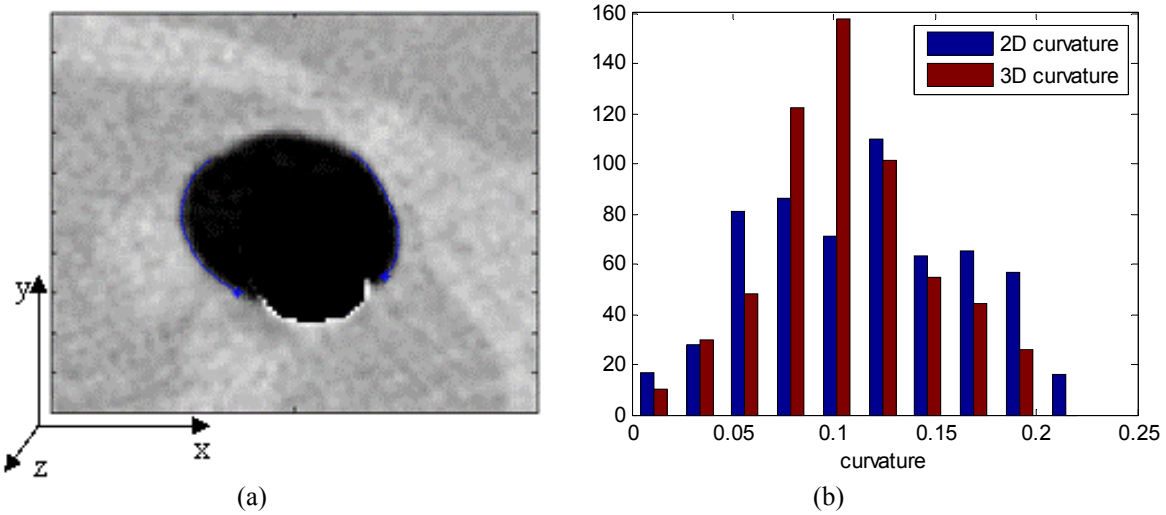

Fig. 9. (a) A slice of the unprepared colon with the tagged material and air-stool PV removed according to the steps explained in Sections 3.1 and 3.2. (b) The histogram of the 2D and 3D curvatures.

After performing the detagging steps of Sections 3.1 and 3.2, visual inspection reveals that the colon wall is receded where it is touching stool (Figure 9 (a)). We now reconstruct the missing part of the colon wall using the curvature information from the known colon wall (the blue curve in Figure 9 (a)). The left boundary (LB, Figure 10 left) is extended (the red curve) until it reaches the right boundary (RB) as a reconstruction of the missing boundary as follows:

- The starting slope matches the slope of end point of LB.
- The starting curvature is the average curvature of the end points of the LB.
- The curvature is changed linearly such that it reaches the first point of RB.

Similarly, another curve (the green curve in Figure 10 right) is calculated by starting from the right boundary (RB). The two red and green curves are weighted and averaged. The weight changes such that at left the red curve contributes more and at the right the green curve. Another weight is applied based on how the ending slope matches the slope of the known boundary: the curve whose ending slope matches the starting slope of the known boundary has higher weight.

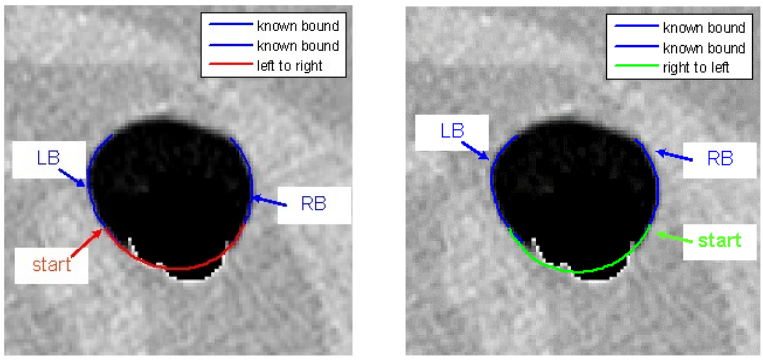

Fig. 10. LB and RB refer to the known Left Boundary and Right Boundary respectively. In the left image, the reconstructed curve (red curve) is generated from left to right, and in the right image the reconstructed curve (green) is generated from right to left.

Figure 11 shows the reconstruction of the missing boundary in different CT slices. The missing bottom part is reconstructed from the known boundary on the left and right. The curves generated from left to right (red) and from right to left (green) are very close to each other in five slices. This may suggest that the constant curvature model is to some degree legitimate.

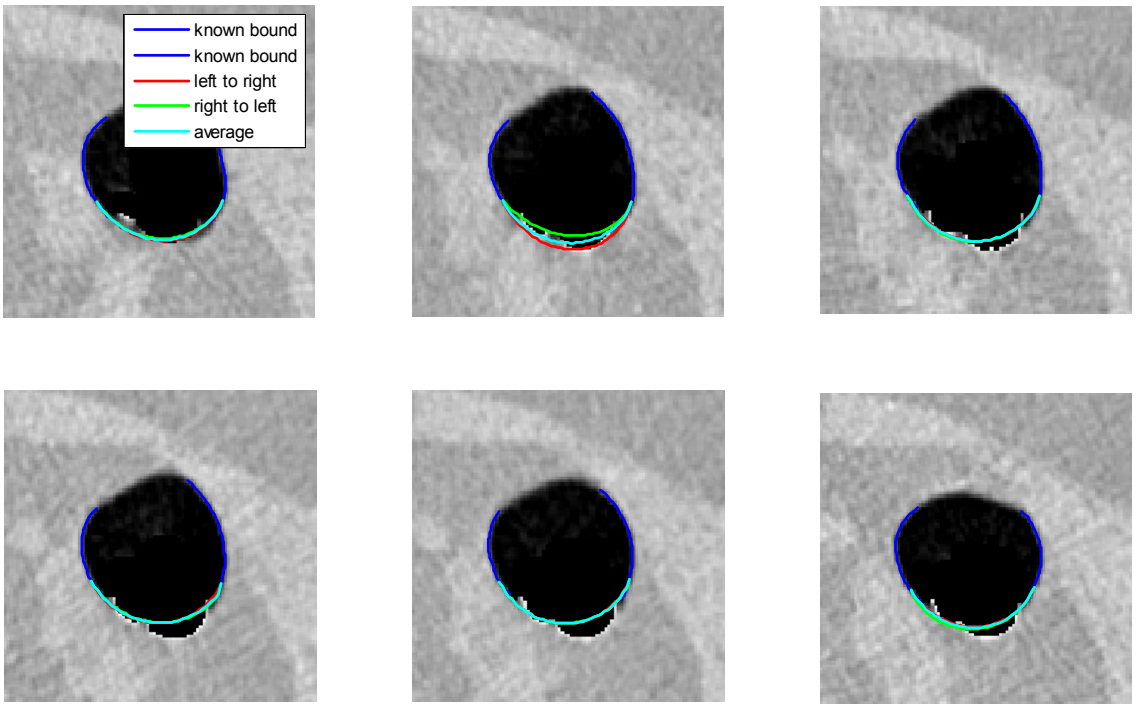

Fig. 11. Six CT slices of patient data with solid preparation after performing the detagging steps of Sections 3.1 and 3.2. The blue curves on the left and right of the colon wall show the known boundary, from which the missing part in the bottom is reconstructed. The reconstructed curves generated from left to right and from right to left are in red and green respectively as marked in the top left image. The curve generated from averaging the two red and green curves is in cyan. The three red, green and cyan curves almost match in five slices and can only be distinguished in the top middle image, suggesting that the reconstruction method is well behaved.

We can now measure how much the tagging material causes the colon wall to withdraw from its original position. Figure 12 shows the average HU of the tagging material versus the displacement of the colon wall (the longer curve in blue). The HU is averaged over an area close to the colon wall where the displacement is measured. Visual inspection suggests that the displacement is too high for pseudo-enhancement alone.

We hypothesize that the weight of the stool also contributes to the withdrawal of the colon wall. To test this hypothesis, we search for parts of the colon where stool is attached to the top part of the colon wall. The stool at these locations is light enough not to fall due to gravity. We then perform the detagging steps of Sections 3.1 and 3.2 and measure the displacement versus HU of the tagged material. The red curve in Figure 12 shows the displacement, verifying that the deformations of the colon wall due to gravity is not negligible compared to the deformations due to the air pressure applied. These results also provide information for decoupling of the two contributors to the colon wall deformation.

As we emphasized before, the curvature prior do not hold in all parts of the colon. It entirely fails in parts of the colon with folds. Therefore, this is not a reconstruction method. It can be used in parts of the colon without any fold to provide parameters required for pseudo-enhancement correction. These parameters depend on the HU of the tagging material and on the CT imaging unit used. Therefore, it can substitute phantom based calibration proposed in [17].

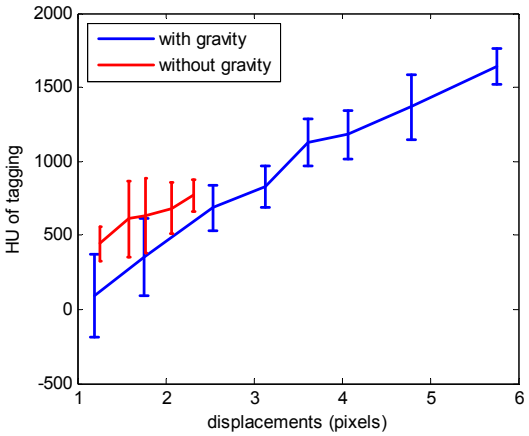

Fig. 12. The displacement and corresponding standard deviation in the colon wall versus the HU of the tagging material. HU is averaged in 3D over a neighborhood close to where the displacement is measured. The blue curve shows the total displacement caused by pseudo-enhancement and gravity, and the red curve shows the displacement only caused by pseudo-enhancement (where stool is connected to the top part of the colon wall).

4. DISCUSSION AND CONCLUSION

We presented two novel physics-based models that can be useful in ECC and in CAD of polyps. The first model is a differential equation of the shape of the meniscus profile. We tested this model in the patient data and showed that it holds with an acceptable accuracy. The second model can be used for correction of pseudo-enhancement caused by the tagged material. The model is based on the fact that a homogenous, isotropic and thin pressured membrane has constant average curvature. We then manually selected parts of the colon where no folds exist (to satisfy the requirement of being thin and homogenous everywhere) and assumed that the curvatures should have small variance across the colon wall. We used this model to reconstruct parts of the colon wall that are in contact with the tagged material, where pseudo-enhancement causes the colon wall to appear receded. The recession is visible in Figure 9, 10 and 11. The amount of recession in these figures looks too high to be caused just by pseudo-enhancement. We proposed that this recession is partly caused by gravitational force of the stool on the colon wall. We proposed an experiment comparing the recession of the colon wall in two cases: (1) where large pieces of stool (and therefore large gravitational force) is resting on the

bottom parts of the colon wall and (2) where small pieces are attached the top parts of the colon wall and has not fallen down due to gravity. The results in Figure 12 show that the apparent displacement in the colon wall is caused by two factors of pseudo-enhancement and gravitational forces. This experiment provides means to decouple the effect of each of these factors and to measure the effect of the pseudo-enhancement as a function of the tagging material's HU. We propose using this measurement to eliminate the need for phantom experiment proposed in [17] for pseudo-enhancement correction. Future work will focus on validation of the proposed method, specifically comparing the results with the phantom-based method proposed in [17]. The method proposed in Section 3.3 uses 2D curvatures for 2D (slice by slice) curve reconstruction. A 3D method where 3D curvatures are used and surfaces are reconstructed is also the subject of future work.

REFERENCES

[1] Sidney J, Winawer M. Screening of colorectal cancer. Surg Oncol. 2005; 14:699-722

[2] Winawer S et al. Prevention of colorectal cancer by polypectomy. The National Polyp Study Workgroup. N. Eng. J Med 1993; 329:1977-1981

[3] Pickhardt P and Choi JHR. Electronic Cleansing and Stool Tagging in CT Colonography: Advantages and Pitfalls with Primary Three-Dimensional Evaluation. AJR. 2003; 181:799-805

[4] Li L et al. An Image Segmentation Approach to Extract Colon Lumen through Colonic Material Tagging and Hidden Markov Random Field model for virtual colonoscopy. SPIE. 2002; 4683:406-411

[5] Wang Z et al. An Improved Electronic Colon Cleansing Method for Detection of Colonic Polyps by Virtual Colonoscopy. IEEE Trans. Biomed. Eng. 2006; 53:1635-1646

[6] Le Lu, Adrian Barbu, Matthias Wolf, Jianming Liang, Marcos Salganicoff, and Dorin Comaniciu, Accurate Polyp Segmentation for 3D CT Colonography Using Multi-Staged Probabilistic Binary Learning and Compositional Model. IEEE Conference on Computer Vision and Pattern Recognition, June, 2008, Anchorage, USA

[7] M Wolf, P Cathier, S Lakare, M Dundar, L Bogoni Efficient detection of polyps in CT colonography Proceedings of SPIE 2007 San Diego, USA

[8] Yao J et al. Colonic polyp segmentation in CT colonography-based on fuzzy clustering and deformable models. IEEE Trans. Med. Imag. 2004; 23:1344-1352

[9] Yao J and Summers RM. Adaptive deformable model for colonic polyp segmentation and measurement on CT colonography. Med. Phys. 2007; 34:1655-1664

[10] Cehn et al. A novel approach to extract colon lumen from CT images for virtual colonoscopy. IEEE Trans. Med. Imag. 2000; 19:1220-1226

[11] Nappi, J. and Yoshida H. Fully Automated Three-Dimensional Detection of Polyps in Fecal-Tagging CT Colonography. Acad. Rad. 2007; 14:287-300

[12] Lee SL and Lee HD. Evolution of liquid meniscus shape in a capillary tube. ASME J. Fluids Eng. 2007; 129:957-965

[13] Lefere P, Gryspeerdt S, Dewyspelaere J, Baekelandt M and Van Holsbeeck B. Dietary Fecal Tagging as a Cleansing Method before CT Colonography: Initial Results—Polyp Detection and Patient Acceptance; Radiology, 2002; 224:393

[14] Carston M, Wentz R, Manduca A and Johnson D. CT colonography of the unprepared colon: an evaluation of electronic stool subtraction SPIE Medical Imaging, 2005; 5746:424-431

[15] Johnson D, Manduca A, Fletcher J, MacCarty R, Carston m, Harmsen S and Mandrekar J. Noncathartic CT Colonography with Stool Tagging: Performance With and Without Electronic Stool Subtraction AJR 2008; 190:361-366

[16] S Lakare, M Wan, M Sato, A Kaufman 3 D digital cleansing using segmentation rays. IEEE Visualization 2000

[17] Nappi J and Yoshida H. Adaptive correction of the pseudo-enhancement of CT attenuation for fecal-tagging CT colonography. Medical Image Analysis 2008; 413-426

[18] Gere J and Goodno B. Mechanics of Materials 2008

[19] Pressley A. Elementary Differential Geometry, Springer 2001